

Severely dystrophic axons at amyloid plaques remain continuous and connected to viable cell bodies

Robert Adalbert,¹ Antal Nogradi,² Elisabetta Babetto,¹ Lucie Janeckova,¹ Simon A. Walker,¹ Martin Kerschensteiner,³ Thomas Misgeld⁴ and Michael P. Coleman¹

1 The Babraham Institute, Babraham Research Campus, Babraham, Cambridge, CB22 3AT, UK

2 Laboratory of Neuromorphology, Department of Ophthalmology, University of Szeged, H-6720 Szeged, Hungary

3 Institute of Clinical Neuroimmunology, Ludwig-Maximilians University, Munich, Germany

4 Institute of Neuroscience, Technical University Munich, Munich, Germany

Correspondence to: Dr Michael Coleman,
B540, The Babraham Institute,
Babraham Research Campus, Babraham,
Cambridge, CB22 3AT, UK
E-mail: michael.coleman@bbsrc.ac.uk

Synapse loss precedes cell death in Alzheimer's disease, but the timing of axon degeneration relative to these events, and the causal relationships remain unclear. Axons become so severely dystrophic near amyloid plaques that their interruption, causing permanent loss of function, extensive synapse loss, and potentially cell death appears imminent. However, it remains unclear whether axons are truly interrupted at plaques and whether cell bodies fail to support their axons and dendrites. We traced TgCRND8 mouse axons longitudinally through, distal to, and proximal from dystrophic regions. The corresponding neurons not only survived but remained morphologically unaltered, indicating absence of axonal damage signalling or a failure to respond to it. Axons, no matter how dystrophic, remained continuous and initially morphologically normal outside the plaque region, reflecting support by metabolically active cell bodies and continued axonal transport. Immunochemical and ultrastructural studies showed dystrophic axons were tightly associated with disruption of presynaptic transmission machinery, suggesting local functional impairment. Thus, we rule out long-range degeneration axons or dendrites as major contributors to early synapse loss in this model, raising the prospect of a therapeutic window for functional rescue of individual neurons lasting months or even years after their axons become highly dystrophic. We propose that multi-focal pathology has an important role in the human disease in bringing about the switch from local, and potentially recoverable, synapse loss into permanent loss of neuronal processes and eventually their cell bodies.

Keywords: Alzheimer's disease; axonal dystrophy; axonal damage signalling; TgCRND8; synapse dysfunction

Abbreviations: A β = amyloid (β peptide); APP = amyloid precursor protein; CFP = cyan fluorescent protein; ex. = excitation; em. = Emission; YFP = yellow fluorescent protein

Introduction

Focal axon and dendrite dystrophy around amyloid plaques is prominent in Alzheimer's disease and occurs early in mouse

models of familial Alzheimer's disease (Onorato *et al.*, 1989; Dickson *et al.*, 1999; Tsai *et al.*, 2004; Brendza *et al.*, 2005; Spires *et al.*, 2005; Adalbert *et al.*, 2007) but the role of dystrophic neurites in pathogenesis remains enigmatic a century

after they were described (Fischer, 1907). Dystrophic axons and dendrites are ideally placed to mediate both amyloid beta protein (A β) toxicity through this direct association with plaques, and also the elusive link to tau, an axonal protein (Dickson *et al.*, 1999; Adalbert *et al.*, 2007). Recent data suggest that dystrophic axons and dendrites are more than an epiphenomenon in Alzheimer's disease pathogenesis. Reports of axon and dendrite interruption at amyloid plaques (Phinney *et al.*, 1999; Tsai *et al.*, 2004; Grutzendler *et al.*, 2007) and loss of dendritic spines (Tsai *et al.*, 2004; Spires *et al.*, 2005; Grutzendler *et al.*, 2007) suggest mechanisms linking dystrophy to early synapse loss in patients (Selkoe, 2002). Moreover, despite the importance of synapse loss for early symptoms, synapse loss is a localized, potentially reversible event. It is equally important to understand key steps to irreversible neuron damage, such as axon interruption and cell death, as beyond this point the potential for therapy to reverse cognitive decline will be severely curtailed. We hypothesized that axonal dystrophy is well placed to trigger axon interruption and potentially cell death as well as synapse loss, placing it at the centre of a parsimonious model for Alzheimer's disease pathogenesis. Thus, we aimed to understand how axonal dystrophy fits into the wider sequence of events that take place in the Alzheimer's disease brain.

Synapses are sites of both A β toxicity (Lacor *et al.*, 2007) and A β release (Lazarov *et al.*, 2002; Sheng *et al.*, 2002) but they are unlikely to be the only sites for either, and it remains unclear how synapse loss relates to the more clearly irreversible steps of axonal interruption and cell death. Blocking axonal transport exacerbates total A β load (Stokin *et al.*, 2005), and plaques occur in axonal tracts with little or no synaptic input (Wirths *et al.*, 2006). Axonal release of A β could explain each of these observations, whereas neither fits well with A β release solely at synapses. Moreover, the first site of cellular degeneration is often a poor indicator of where neuronal damage first occurs (Conforti *et al.*, 2007). Thus, A β -induced synapse loss could, at least in part, be mediated by remote, dystrophic damage to axons and dendrites. In particular, axotomy experiments show that the reported interruption of axons at amyloid plaques (Phinney *et al.*, 1999; Tsai *et al.*, 2004) should trigger presynaptic terminal loss within hours (Miledi and Slater, 1970), followed by postsynaptic spine loss (Fiala *et al.*, 2002), and cell death some time later (Berkelaar *et al.*, 1994; Koliatsos *et al.*, 1994; Fishman and Parks, 1998). Mice may not live long enough to show extensive cell death, but identifying those specific cell bodies whose axons are damaged should at least reveal some early responses to an axonal damage signal. Dendritic damage may also trigger cell death, as extensive branching of dendritic trees increases the likelihood of neuronal death following chronic A β exposure (Capetillo-Zarate *et al.*, 2006). Unfortunately, how, when and indeed whether axon and dendrite dystrophy at amyloid plaques affects other compartments of the same neuron remains unknown (Adalbert *et al.*, 2007).

A block of axonal transport can also cause 'dying back' axon degeneration (Ferri *et al.*, 2003; Coleman, 2005) and cell death (LaMonte *et al.*, 2002; Hafezparast *et al.*, 2003). As A β blocks axonal transport (Rui *et al.*, 2006) and amyloid plaques are associated with organelle accumulation and cytoskeletal disruption

(Phinney *et al.*, 1999; Boutajangout *et al.*, 2004) axonal transport is likely to be impaired at plaques. This too could explain synapse loss, as blocking axonal transport causes nerve terminal withdrawal even while axonal structure is retained (Hudson *et al.*, 1984). However, whether transport is completely blocked at amyloid plaques, triggering distal axon degeneration, remains unknown.

To test the hypothesis that dystrophic axons and dendrites are precursors of irreversible neuron damage, we traced them back to their cell bodies in double hemizygous TgCRND8/YFP-H mice. TgCRND8 mice inherit a highly aggressive amyloidopathy caused by expression of double mutant amyloid precursor protein (APP; K670N/M671L plus V717F) (Chishti *et al.*, 2001), leading to early dystrophic neurites and some cell death (Bellucci *et al.*, 2006). However, the temporal relationship between neurite dystrophy and cell death has not been studied. YFP-H mice express yellow fluorescent protein (YFP) from a Thy1.2 promoter in a subset of neurons (Feng *et al.*, 2000), greatly facilitating longitudinal axon and dendrite imaging (Beirowski *et al.*, 2004, 2005; Coleman *et al.*, 2005; Enright *et al.*, 2007) and detection of axonal dystrophy (Bridge *et al.*, 2007). Thus, as well as tracing dystrophic axons back to the corresponding neurons, this enabled us to use axon and dendrite continuity, dendritic spines and branching, and nuclear size and location as functional markers of that cell's survival.

Surprisingly, we found that almost all TgCRND8 axons retain continuity throughout the disease course, even at sites of extreme dystrophy. The corresponding cell bodies were morphologically normal, with unaltered nuclear size, and likely to be metabolically active as evidenced by their support for both axons and dendrites. However, synaptic boutons in dystrophic axons show loss of essential components for synaptic transmission, indicating a key role for the presynaptic compartment in early pathogenesis. Dystrophic apical dendrites at amyloid plaques also connected to normal appearing cell bodies that supported their basal dendrites and axon. Intriguingly, some dystrophic axons developed morphologically distinct secondary swellings up to 16 μ m proximal to amyloid plaques, suggesting cumulative impairment of function.

Experimental procedures

Mouse origins and breeding

Hemizygous male TgCRND8 mice (Chishti *et al.*, 2001) on a 50:50 C57BL/6:129Sv background were bred to female Thy1.2-YFP-H homozygotes on a C57BL/6 background (Feng *et al.*, 2000) to produce double hemizygous TgCRND8/YFP-H in the F1 generation, which were genotyped by Southern blotting. On this genetic background pathology develops rapidly in TgCRND8 mice and there is ~30% mortality by 6 months of age. Some double hemizygous TgCRND8/YFP-H were crossed with MitoS and MitoP mice, which express cyan fluorescent protein (CFP) targeted specifically to neuronal mitochondria (Misgeld *et al.*, 2007). The double hemizygous TgCRND8/YFP-H and triple hemizygous TgCRND8/YFP-H/MitoS or P were genotyped by Southern blotting. All animal experiments were performed under the UK Animals (Scientific Procedures) Act 1986 and according to

Project Licence 80/1778, or with the approval of the Committee for Animal Experiments, University of Szeged regarding the care and use of animals for experimental procedures (Licence number: VII./5027/002/2003).

Tissue preparation

TgCRND8 mice with YFP-H and/or Mito-S or -P, together with corresponding non-TgCRND8 littermate controls between 2- and 6-month-old were perfused transcardially under sodium pentobarbital terminal anaesthesia with 4% phosphate-buffered paraformaldehyde. Dissected brains were postfixed by immersion in the same fixative for 3 h at 4°C and then cryoprotected in 30% sucrose in phosphate-buffered saline (PBS) at 4°C. Sagittal brain sections were cut at 50 µm using a Leica CM 1850 cryostat. For synaptophysin immunohistochemistry the sections were cut at 40 µm.

Immunohistochemistry and staining

Sections were incubated in blocking buffer containing 0.5% Triton X-100 and 3% normal goat serum in tris-buffered saline (TBS) for 1 h at room temperature followed by incubation in primary antibody diluted in blocking buffer overnight at 4°C. The following primary antibodies were used at the specified dilutions: rabbit anti-pan Aβ (Biosource, 1:1000), mouse anti-APP A4 (Clone 22C11, Chemicon, 1:200) and mouse anti-synaptophysin (clone SY38, Dako, 1:100). After incubations in primary antibodies all sections were rinsed in TBS and then incubated with Alexa Fluor 568 goat anti-rabbit or goat anti-mouse IgG secondary antibodies (Invitrogen-Molecular Probes, at 1:250 dilution) for 2 h at room temperature. After extensive washing in TBS the sections were mounted for epifluorescence and confocal microscopy in Vectashield Mounting Medium (Vector Laboratories). To stain fibrillar amyloid deposits some sections were incubated in 0.02% Thioflavine S in TBS for 10 min and then rinsed in 50% ethanol in TBS and 100% TBS before mounting. For nuclear staining most sections were stained with 0.2% Hoechst 33258 dye (Invitrogen-Molecular Probes) in 0.1% TritonX-100 in TBS, washed extensively in TBS and then mounted in Vectashield Mounting Medium. Some sections were directly mounted in Vectashield Mounting Medium containing DAPI. To quantify YFP positive neurons in cortical layer V, sections were stained with NeuroTrace fluorescent Nissl stain (Invitrogen-Molecular Probes, 1:300) for 20 min. After extensive washing in TBS for 2 h at room temperature, the sections were mounted in Vectashield.

Imaging

Within the cortex, YFP-H mice express YFP in only a small subset of layer V neurons. This makes it possible to trace their axons and dendrites as far as the corpus callosum and apical tufts respectively. Therefore, we focussed on the axons and dendrites of layer V neurons that encountered amyloid plaques within the cortex. Moreover, imaging at lower laser intensity reveals nuclear size, shape and location as an additional indicator of the state of health of the cell body.

The stained sections were imaged with a Zeiss LSM 510 META laser scanning confocal microscope using a 40× NA 1.3 or 63× NA 1.4 oil immersion objective. Neuronal structures and amyloid plaques were scanned using a multi-track configuration with laser excitation (ex.) lines and emission (em.) filters as follows: DAPI/Hoechst 405 nm ex. 420–480 nm em., CFP 405 nm ex. 470–500 nm em., Thioflavine S 405 nm ex. 475–525 nm em., YFP 488 nm ex. 505–550 nm em., AlexaFluor 568 and NeuroTrace 561 nm ex. 575–615 nm em. Single confocal slices or z-stacks at 0.4–0.5 µm steps were acquired to generate the data images. Three-dimensional reconstructions of confocal slices were made using Volocity software (Improvision). Conventional fluorescence imaging was carried out using an Olympus IX 81 inverted microscope coupled to an Olympus U-TV0.5XC digital camera system.

Quantitative analysis

Nuclear size was measured using Zeiss LSM Image Browser software. The number of amyloid plaques stained with Thioflavine S was determined in the same cortical regions where we based our axon studies, those where axon imaging is most clear. Six sagittal sections (3 sections/hemisphere) were made at 1.5, 1.0 and 0.5 mm, respectively from the midline (or interhemispheric fissure). A 90 mm² box was systematically randomly placed within six sagittal sections of frontal, parietal and occipital cortex and plaques counted and measured within it (excluding satellite plaques). Temporal cortex was excluded from this analysis as axons in this region cannot be followed back to their cell bodies. The diameter of the plaques (single line measurement) was measured using AnalySIS software (Olympus). Amyloid plaques with dystrophic YFP axons were quantified in 2 month and 5–6 month old mice. In both age groups 30 amyloid plaques were counted. In the 2-month-old mice average sized plaques were quantified, and at 6 months the largest plaques (40–70 µm) were quantified. Secondary swellings were quantified in both cortical hemispheres in the first 400 µm from the interhemispheric fissure. Here, the axons could be followed over long distances from the cell body to corpus callosum on sagittal sections.

Synaptophysin immunohistochemistry was quantified in the cortex in two sections per animal located 1 mm from the midline. Immunolabeled sections were imaged with a Zeiss LSM 510 META laser scanning confocal microscope. Single confocal slices were acquired to generate the data images using the same system settings for all samples. For each TgCRND8 mouse synaptophysin levels were assessed in and around 10 plaques chosen by systematically random sampling. For each plaque, three 500 µm² areas were systematically randomly sampled within the fibrillar plaque region and three more immediately adjacent to it. Similar procedures were applied to a control mouse (Supplementary Fig. 8). The average pixel intensity of synaptophysin staining was calculated for each image using Zeiss LSM Image Browser software. Some z-stacks at 0.3 µm steps were also acquired to generate qualitative data images. YFP positive and NeuroTrace positive neurons were quantified in the frontal, parietal, occipital and temporal cortex on single confocal slices of sections spaced 300 µm apart.

The number of axodendritic synapses formed by axons (both dystrophic and normal appearing) was determined by electron microscopy in the area of the plaques and within the equivalent cortical layer (layer IV) of control mice. Five hundred axons were analysed in both sample groups and the numbers of axodendritic synaptic structures formed by these axons were determined. In case of plaques not only intact-looking synapses were counted but all axodendritic synapse-like connections which featured at least the postsynaptic density and synaptic cleft.

Electron microscopy

Double hemizygous mice and TgCRND8 negative, YFP-H positive littermate controls were perfused transcardially under sodium pentobarbital terminal anaesthesia with 4% phosphate-buffered paraformaldehyde and 2.5% glutaraldehyde, pH 7.4. After dissection, cortical samples were extensively washed in 0.1 M phosphate buffer before post-fixation in 1% osmium tetroxide for 2 h. Following dehydration through an ascending series of ethanol solutions and propylene oxide, the nerve segments were embedded in Durcupan resin (Fluka) and cured for 48 h at 60°C. Semithin and ultrathin section were cut on an Ultracut-R ultramicrotome (Leica Microsystems). The ultrathin sections were treated with uranyl acetate and lead citrate and investigated in a JEOL JEM 1010 electron microscope.

Transcallosal lesions

For transection lesions, adult male heterozygous YFP-H mice ($n=8$) were anaesthetized with Hypnorm (0.0045 ml/10 g body weight) and Diazepam (0.0075 ml/10 g). A 4 mm \times 6 mm craniotomy was carried out in the midline, the dura mater was exposed and cut along the left side of the craniotomy. The dura mater was then carefully pulled to the right side without damaging the superior longitudinal sinus. A transcallosal axotomy was performed using a tilted knife (Grieshaber 681.45) in the midline extending ~6 mm rostrocaudally. Then the dura mater was pulled back to its original position and the skull was closed with a small piece of wet TissuDura (Baxter International Inc., Vienna, Austria). The skin was closed and the animals were allowed to recover. One to two weeks after surgery the animals were intracardially perfused with 4% phosphate-buffered paraformaldehyde, their brains were removed and immersion fixed overnight in the same fixative and then processed. For colchicine injections ($n=6$), a hole was drilled 1 mm lateral to the sagittal suture on the left side and 2 mm posterior to the bregma. A microliter syringe was filled with either 2 mg/ml ($n=3$) or 6 mg/ml ($n=3$) colchicine dissolved in physiological saline. One microliter colchicine volumes were injected 2 mm deep into the anterior and posterior parts of the corpus callosum at two separate injection sites. The skin incision was sutured and the animals were allowed to survive for 2 days before perfusion.

Statistical analysis

Student's t-test for independent samples (two-tailed) and the Mann–Whitney U-test was used to compare the groups of data.

Results

Reaction of YFP-labelled cortical layer V neurons to experimental axon transection and transport block

Our studies focussed on cortical layer V neurons because restricted expression of the YFP-H transgene in this layer facilitates longitudinal tracing of their processes (Feng *et al.*, 2000; Enright *et al.*, 2007). Axons and dendrites from other layers are not visible, thus simplifying the images. Layer V axons project to corpus callosum, a major site of early axon loss in human Alzheimer's disease (Teipel *et al.*, 2002), and early accumulation of amyloid plaques in both cortex and corpus callosum were previously reported in TgCRND8 mice (Chishti *et al.*, 2001). Moreover, when axons in corpus callosum are experimentally transected, the corresponding neurons in cortex layer V die within 2 weeks (Fishman and Parks, 1998), indicating that this tract was suitable for testing whether axonal interruption in Alzheimer's disease is a cause of neuron death.

In order to establish the appearance of dying YFP-labelled layer V neurons after axon interruption, we first lesioned corpus callosum in YFP-H mice. After 7 days, most pyramidal neurons in cortical layer V were morphologically abnormal in at least one of the following ways (Fig. 1B) none of which was observed in unlesioned tissue (Fig. 1A): irregularly shaped cell body, shrunken, irregularly shaped or sidelined nucleus, absence of clearly stained basal dendrites and axon, truncated apical dendrite and poorly stained cytoplasm. There was massive axonal swelling of corpus callosum axons extending ~1.5 mm either side of the lesion site (Fig. 1E). Similar changes resulted when axonal transport was blocked by colchicine injection into corpus callosum of YFP-H mice. Extensive axon swelling and some axon interruption occurred local to the injection site (Supplementary Fig. 1A) and there was abundant axonal swelling at more distant sites (Fig. 1F). Approximately 25% of the corresponding cell bodies showed nuclear shrinkage and displacement (Fig. 1C). This characterization of axonal and cellular responses to axonal disconnection and transport block indicated what we should expect to see if similar axonal events occurred in the TgCRND8 model. We also confirmed that neurons express YFP in frontal, parietal, occipital (Supplementary Fig. 2) and temporal (not shown) regions of cortex, although there was some variation in the percentage of expressing neurons.

Early pathology: appearance of plaques is followed by small axonal swellings

We then followed the development of amyloid plaques and axonal and dendritic dystrophy in TgCRND8/YFP-H mice aged 2, 3, 4, 5 and 6 months. Significant mortality of unknown cause (Chishti *et al.*, 2001) prevented us from studying older mice on this genetic background, although we did also follow pathology out to 14 months on a different background (see below). Amyloid deposition in TgCRND8 mice is very rapid with the first small

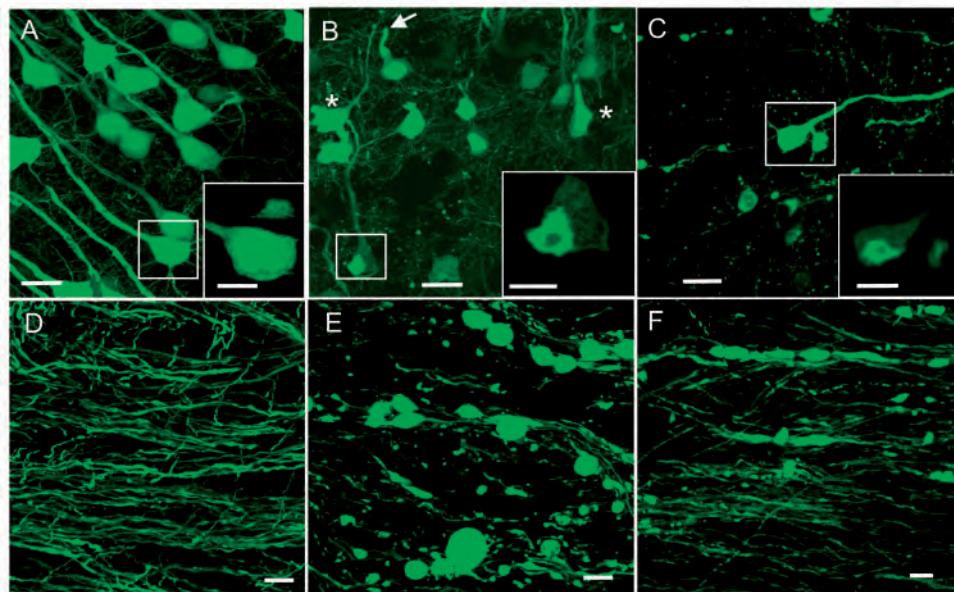


Fig. 1 Morphology of dying YFP-labelled cortical layer V neurons after axon transection and transport block. (A and D) Cortex layer V neurons and corpus callosum axons in untreated YFP-H mice. (B) Dying cortical neurons in YFP-H mice 7 days after transection of their axons in corpus callosum. Cell bodies are irregularly shaped (asterisk) and shrunken, many with sidelined nuclei (inset). Apical dendrites terminate abruptly (arrow) and cytoplasm is poorly stained. (E) Corresponding corpus callosum shows massive axonal swelling on both sides of the lesion. (C and F) Similar changes are seen 2 days after injection of 6 μ g colchicine into corpus callosum. Scale bars: A, B and C: 20 μ m (10 μ m insets); C, D and E: 10 μ m.

plaques appearing in cortex by 2 months, containing both soluble and fibrillar A β . Many axons crossed these early plaques without any signs of dystrophy (Fig. 2A), an observation that was rare at the larger plaques of older mice (see below; Supplementary Table 2). Around one-third of axons at this age showed small, highly focal swellings, sometimes associated with a thickening of the axon just proximal to the plaque, but axon continuity was clearly retained (Fig. 2B; Supplementary Table 2). Thus, axonal dystrophy occurs very early in these mice indicating its potential to contribute to any simultaneous or subsequent events, which include cognitive decline (Chishti *et al.*, 2001).

Axonal swellings become larger but most remain focal

Plaques increased both in number and in size with age (Supplementary Table 1), and axonal dystrophy became an almost universal observation at larger plaques (Supplementary Table 2). The difference between this observation and the recently reported stability in plaque size may reflect the different timescales studied (Meyer-Luehmann *et al.*, 2008). Axonal swellings also became larger, many reaching the size of cell bodies and displaying numerous distortions and mushroom-shaped protrusions (Fig. 3; Supplementary Figs 1 and 3), very similar to those seen in patients (Fischer, 1907; Dickson *et al.*, 1999). Remarkably however, 3D confocal imaging showed these axons remained continuous, not only across dystrophic regions but also distally, and proximally where they connected to morphologically normal cell bodies (Figs 3B–D; 4B and C; Supplementary Figs 3 and 4).

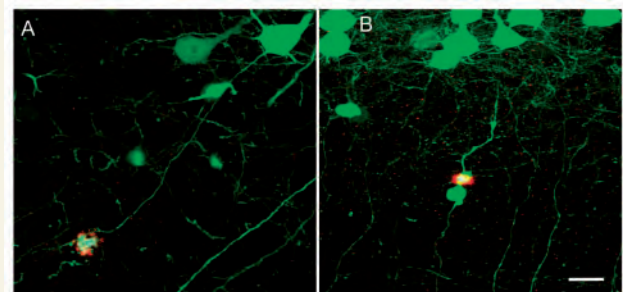


Fig. 2 Early plaque-associated axon pathology. (A) In TgCRND8/YFP-H mice aged 2 months, many axons crossed amyloid plaques containing both soluble and fibrillar amyloid without axonal swelling. (B) However, a few axons showed local swelling and proximal thickening without any interruption of axonal continuity. Figures are representative of nine similar observations at 2 months. Green = YFP; Red = A β deposits; Blue = Thioflavin S. Scale bar: 20 μ m.

Indeed, around 70% of axons were unswollen distal and proximal to plaques, quite indistinguishable from the control axon shown in Fig. 4A. The survival of such structures several months after the onset of axonal dystrophy (Fig. 2B), suggests the presence of both a metabolically active cell body (see below) and bidirectional axonal transport through a continuous axon in the dystrophic region, because failure of either is likely to cause Wallerian degeneration (Fig. 1C) (Ferri *et al.*, 2003; Coleman, 2005). We searched further for signs of axon degeneration in corpus callosum of 5- and 6-month-old mice as an indicator of axon interruption

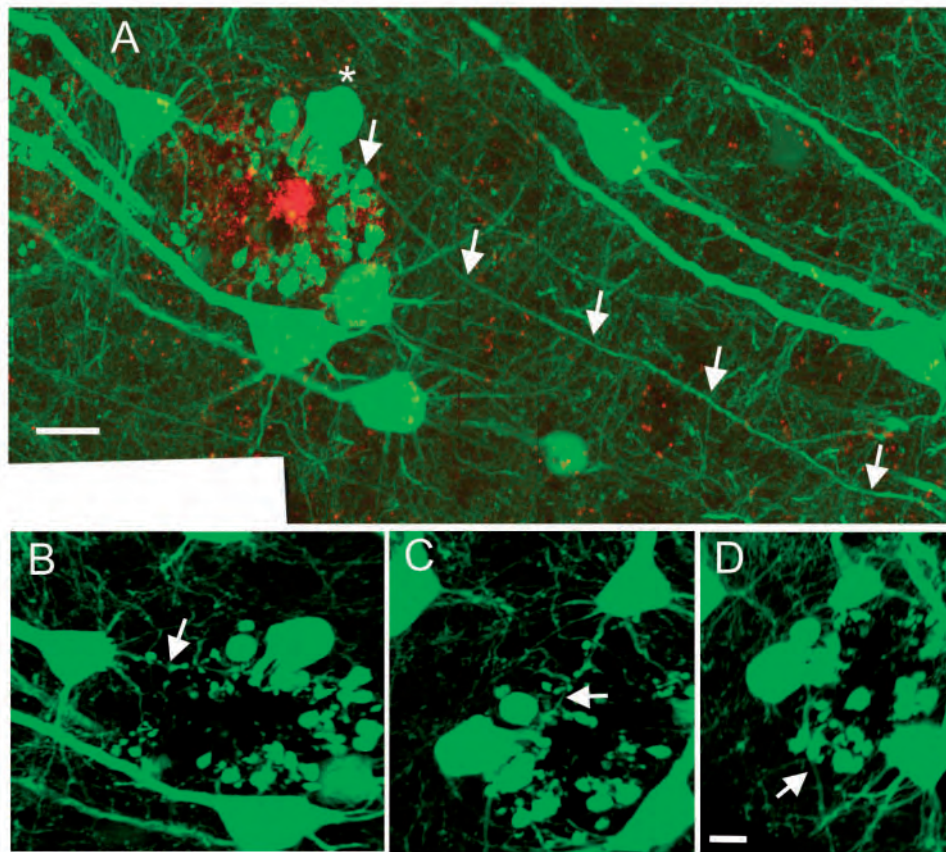


Fig. 3 Axon continuity is retained at even the most severely dystrophic plaques. (A) Axonal dystrophy in a 5-month-old TgCRND8/YFP-H mouse, where axonal swellings reached the size of the corresponding cell body (asterisk). Despite this the corresponding axon remains morphologically normal and continuous distal to the swelling (arrows). Green = YFP; Red = A β deposits; Blue = Thioflavin S. (B, C and D) Rotations of the above image (green channel only) confirm that axonal continuity is retained across the plaque region (arrows) and that this axon is connected to the corresponding cell body. Figure is representative of many similar observations, some of which are shown in Fig. 4 and Supplementary Figs 3 and 4. Scale bar: A: 20 μ m; B, C and D: 10 μ m.

at a more proximal site. In contrast to lesioned corpus callosum (Fig. 1C), the only significant axonal swelling in six TgCRND8/YFP-H mice was close to amyloid plaques (Supplementary Fig. 5).

Not only was axon continuity retained, but these axons were supported by morphologically normal cell bodies whose nuclear size was unaltered even when plaque-associated dystrophy occurred close to the cell body (Fig. 4). Hoechst staining also indicated that neighbouring neurons not expressing YFP also remained healthy, confirming that the YFP labelled population is not unusually resistant and we found no Thioflavin S or phospho tau intraneuronal deposits (data not shown). Similar methods were recently used to assess cell survival in ischemic lesions (Enright *et al.*, 2007). No cells showed the morphological features of neurons with axon transection or transport block (Fig. 1), again suggesting continued delivery of trophic factors by retrograde axonal transport. These neurons also retained the ability to support both the dystrophic axons and the normal complement of basal and apical dendrites. These features suggest a high degree of metabolic activity. Moreover, dendrites of the same cell possessed normal apical tufts and abundant dendritic spines, indicating their likely functionality (Fig. 4B and C). Thus, during several months of pathology, extensive, proximal axonal dystrophy has

no overt effect on axonal continuity, the corresponding cell bodies, or their dendrites.

We were then able to study TgCRND8 mice aged up 14 months by breeding in a component of strain CBA (~12.5%) to the mixed genetic background. This confirmed that the 6 months pathology studied above was not the end-stage in this model and allowed us to follow axonal and cellular events out to a much later timepoint. First, we studied plaque density and size at younger ages, confirming that mice on this background show similar disease onset and progression and that pathology continues to progress beyond 6 months (Supplementary Table 1 and Supplementary Fig. 6). We then studied the pathology in two 14-month-old mice. Remarkably, although axonal dystrophy had become even more pronounced and some axons showed signs of longer range swelling or fragmentation, many axons were still continuous across these sites and unswollen distally, and cell bodies continued to support uninterrupted axons and dendrites (Fig. 4E). We could find no examples of neurons with shrunken and misplaced nuclei resembling those in Fig. 1, although some in the direct vicinity of amyloid plaques appeared squashed (Fig. 8A). Axon swelling was now evident in corpus callosum, although many swellings were clearly continuous with normal axon regions on both sides

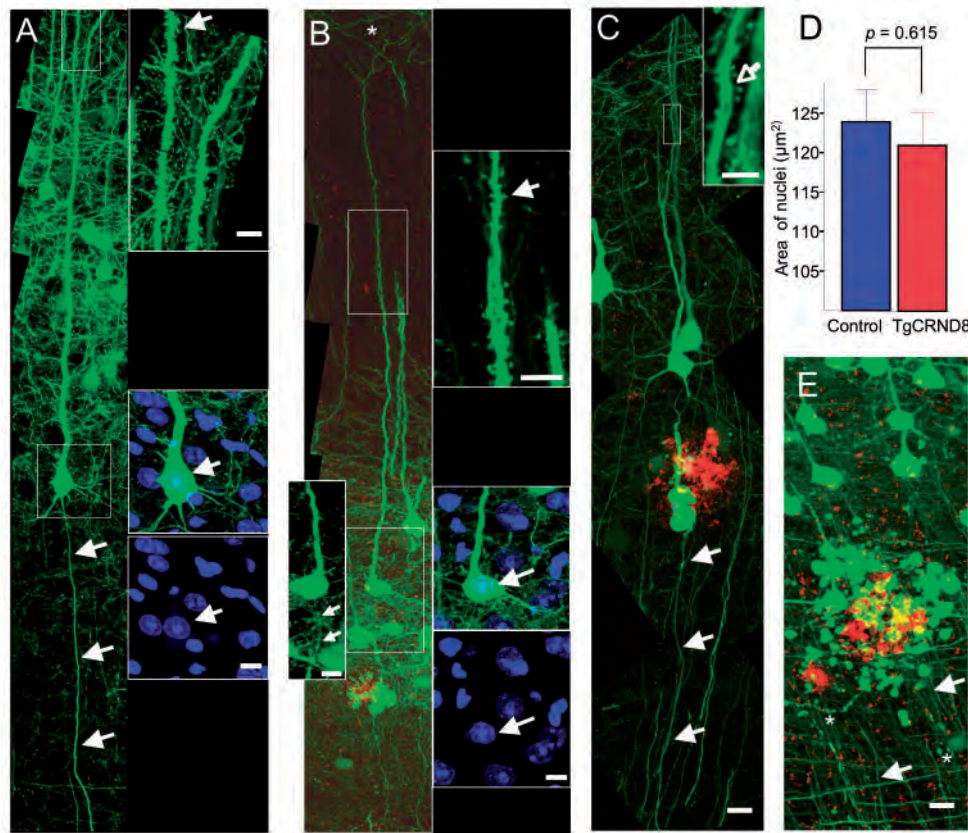


Fig. 4 Axonal dystrophy leaves other parts of the same neuron morphologically unaltered. (A) Cortical neuron from a control YFP-H mouse with boxed areas enlarged on the right, showing expected cell shape, nuclear size (arrow) and dendritic spine density. (B) Cortical neuron from a 5-month-old TgCRND8/YFP-H mouse with severe, proximal axonal dystrophy. Enlarged inset (left) shows a different confocal plane after 180° rotation, where axon continuity is clearly retained. Boxed areas enlarged on the right show similar cell body and nuclear size (arrow, bottom) to A and abundant dendritic spines on apical dendrite (arrow, top), which leads up to normal appearing apical tufts (asterisk main image). (C) Another neuron with severe, proximal axonal dystrophy from a 5-month-old TgCRND8/YFP-H mouse also retains axon continuity and basal dendrites. A branched apical dendrite with abundant dendritic spines is also clearly visible. (D) Quantification (mean \pm SE; $n = 14$) of cross sectional nuclear area reveals no significant difference ($P = 0.615$) between TgCRND8/YFP-H neurons with severe axonal dystrophy within 250 μm of the cell body and control YFP-H neurons. (E) Extensive axonal dystrophy at a plaque in a 14-month-old TgCRND8 mouse. Despite some signs of fragmentation (asterisk) the majority of axons emerging from the dystrophic region are continuous and unswollen (arrows). Cell bodies (top) retain normal morphology and nuclear size and location. Green = YFP; Red = A β deposits; Blue (where present) = Hoechst 33258 dye. Scale bar: A, B, C and E: 20 μm (insets, 10 μm).

(Supplementary Fig. 5), probably an example of dystrophy secondary to axon pathology at other sites (see below). Thus, even 1 year after the onset of amyloid plaques and axonal dystrophy, long-range axon degeneration is very limited compared with just 2 days of colchicine treatment, and cell bodies show no signs of the typical reaction to transport block.

Axonal transport may be partially blocked

The question of how such huge axonal swellings and axonal continuity can coexist prompted us to look more closely at axonal transport in and around the swellings. We hypothesized that transport may be impaired but not completely blocked, a model which in addition to explaining the axonal survival could also

underlie the early loss of synaptic function and structure in Alzheimer's disease as defective axonal transport is a potential cause of synapse loss (Hudson *et al.*, 1984). As direct imaging of transport is not yet feasible in mammalian CNS, we first looked for accumulation of APP, a marker of transport disruption (Ferguson *et al.*, 1997; Medana and Esiri, 2003). Twenty percent of swellings were clearly positively stained for APP, while others, even adjacent swellings in the same axon, were not (Fig. 5A) and similar results were obtained for synaptophysin (17% positively stained) (Fig. 5B). This suggests there are subpopulations of swellings with different degrees of transport impairment, consistent with the partial block model. To rule out artefacts from differential antibody penetration, we then crossed TgCRND8/YFP mice with the recently developed MitoP strain, where mitochondria are specifically and endogenously labelled with cyan fluorescent protein (Misgeld *et al.*, 2007). Swellings in CFP expressing axons were

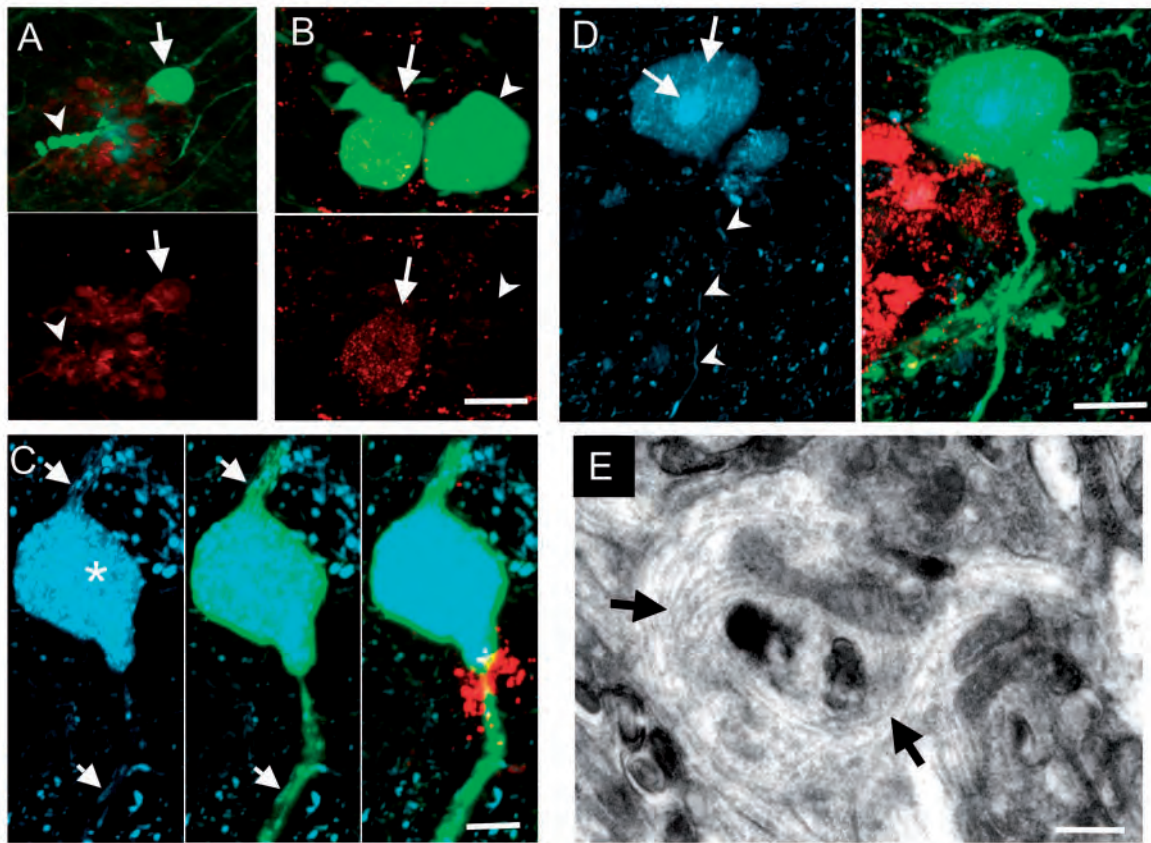


Fig. 5 Partial disruption of axonal transport in TgCRND8 axonal swellings. (A) Some (arrows) but not all (arrowheads) YFP positive axonal swellings stain positively for APP (B) and/or synaptophysin. Note: other APP signal (red) around the plaque in A probably comes from swellings in non-YFP axons. (C) CFP labelled mitochondria in a 6-month-old TgCRND8/YFP-H/MitoP mouse accumulate in swellings but lose their normal morphology (asterisk; see also supplementary figure 9 which shows this more clearly in RGB format). However, on both sides of swellings many mitochondria are elongated (arrows) and typical signs of transport block are missing. (D) Distinct subdomains of variable CFP intensity are often visible (arrows); note again the elongated mitochondria outside the swelling (arrowheads). (E) Apparently continuous microtubules (arrows) enter axonal diverticula in the cortex of a 6-month-old TgCRND8 mouse, providing an ultrastructural correlate for continued, but impaired axonal transport at these swellings. Green = YFP in A, B, C and D; Red = APP staining in A; synaptophysin staining in B; A β deposits in C and D; Blue = Thioflavin S in A; CFP labelled mitochondria in C and D. Scale bar: A: 20 μ m; B and D: 10 μ m; C: 5 μ m; E: 0.2 μ m.

typically CFP positive, indicating mitochondrial accumulation, but 25% of these showed subdomains of variable intensity (Fig. 5C and D) suggesting that the density of mitochondria accumulation differs both between swellings and in different zones of the same swelling (see also Fig. 5E), again consistent with a partial transport block. Moreover, mitochondria immediately distal and proximal to swellings were mostly elongated and well-dispersed, suggesting that there was no major long-term impediment of their transport in these regions (Misgeld *et al.*, 2007). In contrast, within swellings mitochondria are short and rounded, reminiscent of mitochondria after fission. Finally, ultrastructural analysis revealed microtubules diverting into axonal swellings with some adjacent organelle accumulation, but their tracks form parallel whirls and remain uninterrupted for several microns or more (Fig. 5E). In summary, while direct evidence for a partial block of transport at axonal swellings awaits further improvements in live imaging technologies (Misgeld *et al.*, 2007), the current immunocytochemical and ultrastructural data are consistent with a partial block of

axonal transport in dystrophic axons, that may contribute to the growth of the swellings but allows distal axons to survive for significant periods.

Secondary axonal pathology and limited axon interruption

If, as suggested above, axonal transport is only partially blocked at sites of dystrophy, then there is clearly more potential for significant axonal and synaptic damage if several dystrophic sites occur on the same axon, producing a cumulative impairment of axonal transport. Our longitudinal imaging approach allowed us also to identify such multiple swellings on individual axons, with 'secondary' swellings located up to 160 μ m proximal to any plaque-associated dystrophy (Fig. 6A). We suggest that more distant 'secondary' swellings are likely but could not investigate this with these methods. Non plaque-associated swellings have been described previously (Stokin *et al.*, 2005), but their cellular context

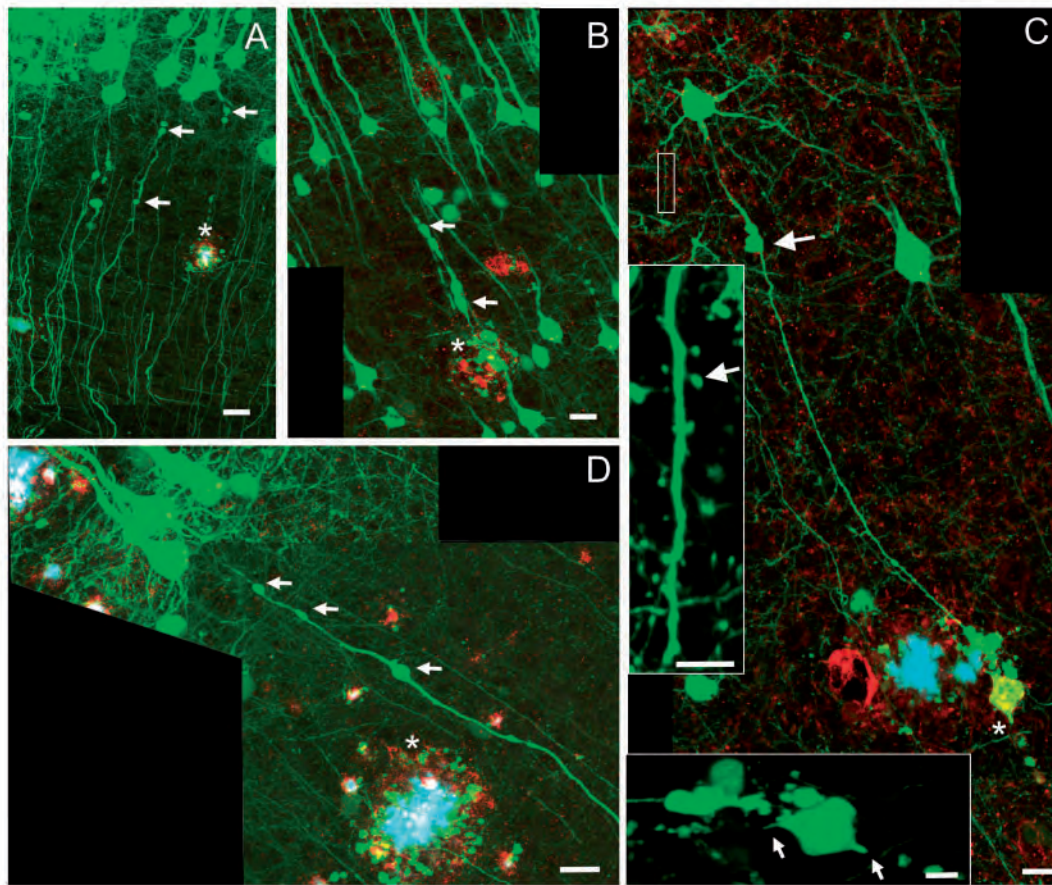


Fig. 6 Secondary axonal dystrophy and axon interruption. (A) Some axons associated with larger plaques (asterisk), and their neighbours, developed secondary swellings away from the plaque (arrows). These were quite symmetrically distributed around the axon shaft, unlike the mushroom-like protrusions sometimes seen at plaques (Figs 3 and 4B). This example is from a TgCRND8/YFP-H mouse aged 4 months. (B) Some axons showed multiple secondary swellings (arrows) proximal to plaques (asterisk), as here in another mouse aged 4 months. These seem likely to disrupt axonal function and ultimately survival more severely than primary dystrophy alone, although most such axons still remained continuous at this stage. (C) The only interrupted axon that was found was in a mouse aged 5 months and has a secondary swelling (arrow) proximal to the plaque (asterisk). Disconnection was confirmed by confocal rotation (arrows in inset, bottom). Despite this, the cell body retained basal dendrites with spines (inset, left). The apparent absence of the apical dendrite is a sectioning artefact. (D) Secondary swellings (arrows) in axons more distant from plaques (asterisk) suggests some radial spreading of A β oligomers. However, the influence of possible more distal plaques, or indeed the one encountered by the dendrite of this neuron (left) cannot be entirely excluded. Green = YFP; Red = A β deposits in A, B and D; APP staining in C; Blue = Thioflavin S. Scale bar: A, B, C and D: 20 μ m (inset, bottom, 10 μ m; inset, left 5 μ m).

has remained unclear. These data show that at least some such swellings occur on axons that have severe plaque-associated dystrophy at other points along their length. Secondary swellings differed from plaque-associated dystrophy in timing and morphology. They were extremely rare at 2 months (only two examples were found) and even in older mice they lacked the asymmetric protrusions, or 'diverticula', prominent around many plaques. At 3, 4, 5 and 6 months 18, 22, 28 and 32% of axons that encountered plaques within the cortex displayed some degree of non-plaque, secondary swelling. In some axons this secondary swelling recurred at multiple sites (Fig. 6B). Despite our expectation that multiple swellings should be more harmful, the large majority of axons with secondary dystrophy also remained continuous, and again the corresponding cell bodies were morphologically normal. However, in mice aged up to 6 months we did find one

single unambiguously interrupted axon, which also had a proximal, secondary swelling (Fig. 6C). Interestingly, even in this cell the corresponding cell body and dendrites did not resemble those after experimental axon transection (Fig. 1), suggesting either that axon continuity had only very recently been interrupted or that an unknown protective mechanism prolongs cell survival when axon continuity is lost in Alzheimer's disease-like pathology.

Synaptic sites on dystrophic axons lack the machinery for normal function

A partial block of axonal transport may not be sufficient to trigger axon degeneration or cell death, but it is well established that the presynaptic machinery is even more sensitive to many types of

axonal impairment than the axon itself (Miledi and Slater, 1970; Hudson *et al.*, 1984; Gillingwater and Ribchester, 2001; Pun *et al.*, 2006). Thus, given the important role of early synapse dysfunction in Alzheimer's disease (Selkoe, 2002), we investigated its association with axonal swellings. Quantitative synaptophysin immunocytochemistry (Fig. 7A) showed a highly significant reduction (Fig. 7B) in signal in the immediate vicinity of plaques, confirming previous reports (Spires *et al.*, 2005; Dong *et al.*, 2007). This depletion largely reflects complete loss of synapses, with only $5.27 \pm 0.38\%$ of axons forming visible synapses in the plaque area compared with $23.12 \pm 1.24\%$ in a similar area from littermate controls. Interestingly, this region of synapse loss is almost exactly limited to the region of neurite dystrophy (Fig. 7C). Moreover, this close spatial association is mirrored by a close temporal association. In 2-month-old mice, precisely when axonal swellings first appear (Fig. 2), synaptophysin depletion too is just becoming detectable (Fig. 7D).

Most importantly, however, electron microscopy revealed 'en passant' synapses lacking the normal machinery for function that were directly associated with axonal swellings but synapsed onto morphologically normal dendrites that retained a post-synaptic density (Fig. 7E–H). These structures probably represent the early stages of synapse loss. Many of these synapses showed few, if any, discernible synaptic vesicles or normal mitochondria (Fig. 7G and H; Supplementary Fig. 7), but instead were filled with large, apparently degenerating organelles of variable electron density. Although functional studies will be needed to confirm the disruption of synaptic transmission, these data show a very close, potentially causative link between axonal dystrophy and disruption of presynaptic machinery.

Heterogeneity of plaque-associated neuronal damage

In principle, presynaptic degeneration could trigger also loss of dendritic spines (Fiala *et al.*, 2002) but although we find it important, our data did not support a model in which deafferentation is the sole cause of postsynaptic abnormalities. First, our electron micrographs also contained examples of abnormal dendrites associated with apparently normal axons (data not shown). Second, longitudinal imaging of affected YFP-H neurons revealed a strikingly heterogeneous pattern of pathology among different neurons. In addition to the dystrophic axons studied above, some neuronal cell bodies directly encountered amyloid plaques and displayed abnormal, often squashed cell morphology and a few lacked obvious dendrites and axons (Fig. s 8A and B). Remarkably, however, even in these circumstances cell death is not rapid because even distorted cell bodies were sufficiently metabolically active to support normal appearing axons and dendrites (Fig. 8B). In other cells it was the dendrites that encountered plaques. As with axon dystrophy, dystrophic apical dendrites remained continuous with no apparent loss of apical tufts, and the corresponding cell bodies showed normal morphology and nuclear size (Fig. 8C). Longitudinal imaging also revealed for the first time that some cells encounter several plaques in different places along their length (Fig. 8D and E). Remarkably, even when both proximal

apical dendrite and axon of the same cell encounter plaques, cell body morphology and continuity can be retained (Fig. 8D). Individual axons can also encounter amyloid plaques more than once (Fig. 8E), a phenomenon that could be even more common in the longer axons of the human brain.

This heterogeneity raises the question of how many neurons are damaged through their axons, how many through their dendrites and how many through their cell bodies. We quantified this in TgCRND8 cortex tracing a $1000\mu\text{m}$ wide path sagittally from the surface of the cortex to the corpus callosum. Within this area, we counted 26 YFP-labelled dystrophic axons, 15 dystrophic dendrites and 7 dystrophic cell bodies. Thus, axonal damage is at least as common as damage to other cellular compartments and considering that the additional path through the corpus callosum and contralateral cortex is not taken into account here, it becomes clear that axonal damage, and the directly associated synapse loss, can make a significant contribution to Alzheimer's disease pathology.

Discussion

We show that 4 months after the onset of axonal dystrophy in this rapidly progressing Alzheimer's disease mouse model, highly dystrophic axons remain continuous and corresponding cell bodies are morphologically unaltered. Even 1 year after plaques and dystrophy arise, affected cortex layer V neurons do not show cell body responses typically induced by experimental axon transection or a block of axonal transport, suggesting that signalling mechanisms communicating axon damage to these cell bodies are not triggered or not fully operative. The ability of TgCRND8 neurons to support long, continuous axons and branched, spiny dendrites suggests they remain metabolically active and that some axonal transport persists despite the extreme nature of the dystrophy. This is important because cell survival and axon and dendrite continuity are the first requirements for functional rescue of individual neurons. However, axonal transport appears to be impaired to some extent and the multiple dystrophic sites we identify on some axons provide scope for a more harmful, cumulative impairment of transport and neuronal function, suggesting this 'secondary dystrophy' represents a more advanced stage of pathology. Moreover, we show that synaptic boutons associated with dystrophic axons lack the normal machinery for synaptic transmission and that axonal dystrophy begins at least as early as synaptophysin depletion. Thus, while Alzheimer's disease pathogenesis is extremely heterogeneous at the individual cell level, a significant proportion of the critical early synapse loss stems from presynaptic disturbances that may be linked to axonal transport defects.

We exclude long-range axonal and dendritic degeneration and axotomy induced cell death as a significant contributors to pathology for many months or even one year after axonal dystrophy arises in TgCRND8 mice. Continuous YFP-labelled axons and dendrites can be traced throughout dystrophic regions, and Wallerian degeneration is absent up to 6 months and rare at 14 months both in the nearby cortex and in corpus callosum where these axons lead (Supplementary Fig. 5).

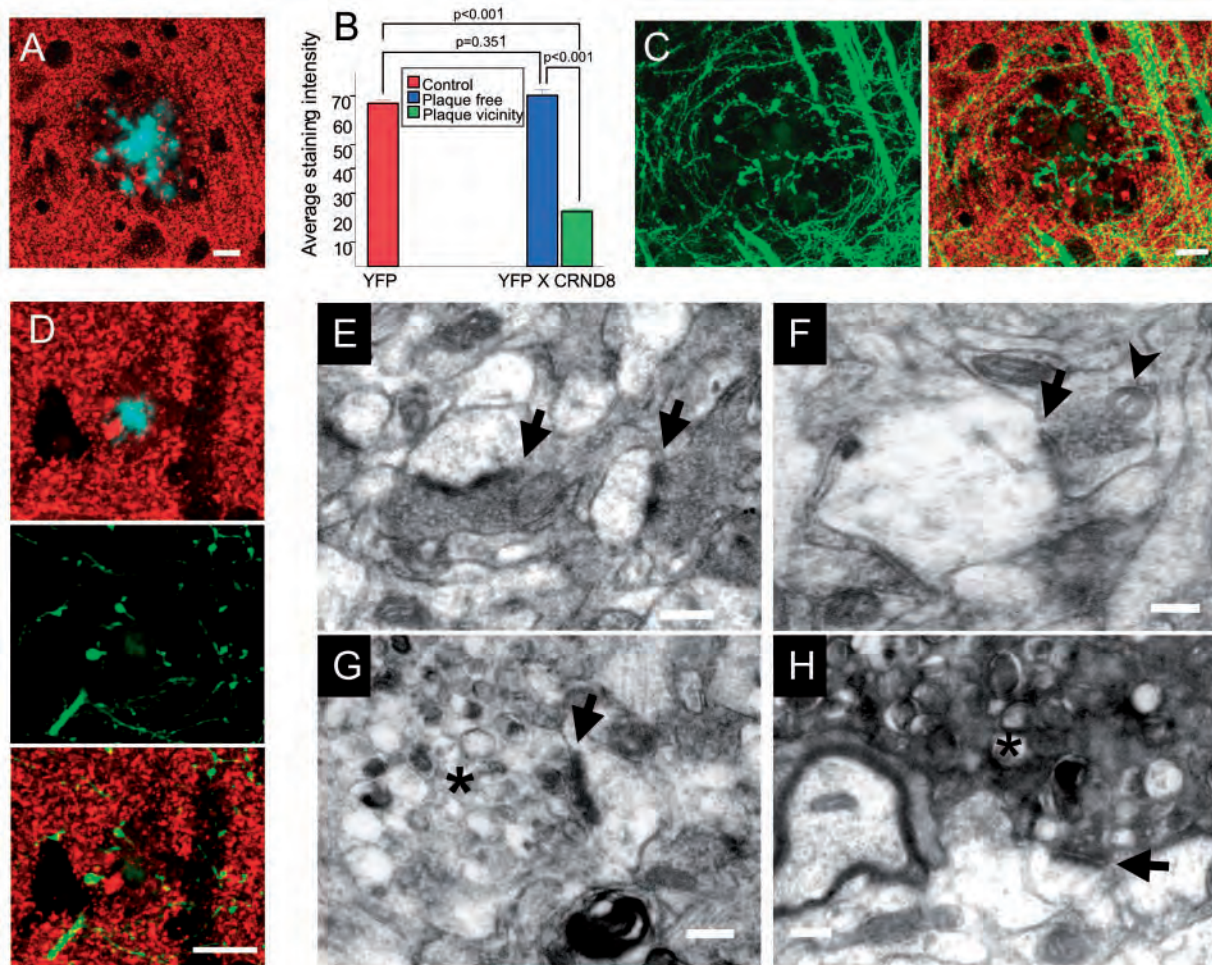


Fig. 7 Axonal swelling is intimately associated with structural disruption of synapses. (A) Synaptophysin immunostaining (red) in a 6-month-old TgCRND8 mouse is depleted around amyloid plaques (blue). (B) Quantification shows this depletion is significant around plaques while other brain regions are unaltered. (C) Interestingly, the zone of synaptophysin (red) depletion corresponds closely with the zone of affected neurites (green) and (E) these features appear at the same stage of pathogenesis, shown here in a 2-month-old mouse (see also Fig. 2). (E–H) Electron micrographs showing normal synapses (arrows) in a wild-type mouse **E** and presynaptic disruption in TgCRND8 **F**, **G** and **H**. We identified four stages of pathology of which three are shown. Each axon synapses with a morphologically normal dendrite with post-synaptic density (arrows). (F) Shows the least severe stage, with subtle, ultrastructural alterations such as swollen mitochondria (arrowhead) but not yet any significant axonal swelling. Synapses formed by these axons appear intact and abundant synaptic vesicles are present. (G) Shows advanced axonal swelling and many more swollen organelles accumulated (asterisk). A few mitochondria remain identifiable, albeit abnormal (not shown) and synaptic vesicles, if present at all, are far less evident and are probably crowded out by these other structures or held back by axonal transport defects. (H) Shows the most severe stage, with a very electron dense presynaptic structure (asterisk), packed with unidentifiable swollen organelles and few or no synaptic vesicles. Remarkably, a wider view shows that this axon is associated with many non-dystrophic dendrites (Supplementary Fig. 7). Red = synaptophysin staining in **A**, **C** and **D**; Blue = Thioflavin S in **A**; Green = YFP in **C** and **D**. Scale bar: **A**, **C** and **D**: 10 μ m; **E**, **F**, **G** and **H**: 0.2 μ m.

Axonal transport is likely to continue to some extent across dystrophic regions to keep distal and proximal structures alive. Defective axonal transport triggers Wallerian-like axon degeneration (Ferri *et al.*, 2003) and cell death (LaMonte *et al.*, 2002; Hafezparast *et al.*, 2003; Martin *et al.*, 2006) and characteristic responses to axon damage in surviving cells (Fig. 1). Nevertheless, accumulation of APP, synaptophysin and mitochondria in some axon swellings, together with the diversion of microtubule tracks away from the main axis of the axon does suggest some impairment of axonal transport (Fig. 5).

Drosophila kinesin and dynein mutants provide an interesting precedent for a partial blockade. Their axons develop organelle-filled swellings but mitochondria can both enter and leave these swellings (Pilling *et al.*, 2006). One possible cause of a transport defect is A β (Rui *et al.*, 2006). If a partial transport defect allows more time for axonal APP processing as suggested (Stokin *et al.*, 2005) this could generate more A β , feeding back into a worsening transport defect and progressive enlargement of both amyloid plaques and dystrophy (Figs 2 and 3; Supplementary Table 1).

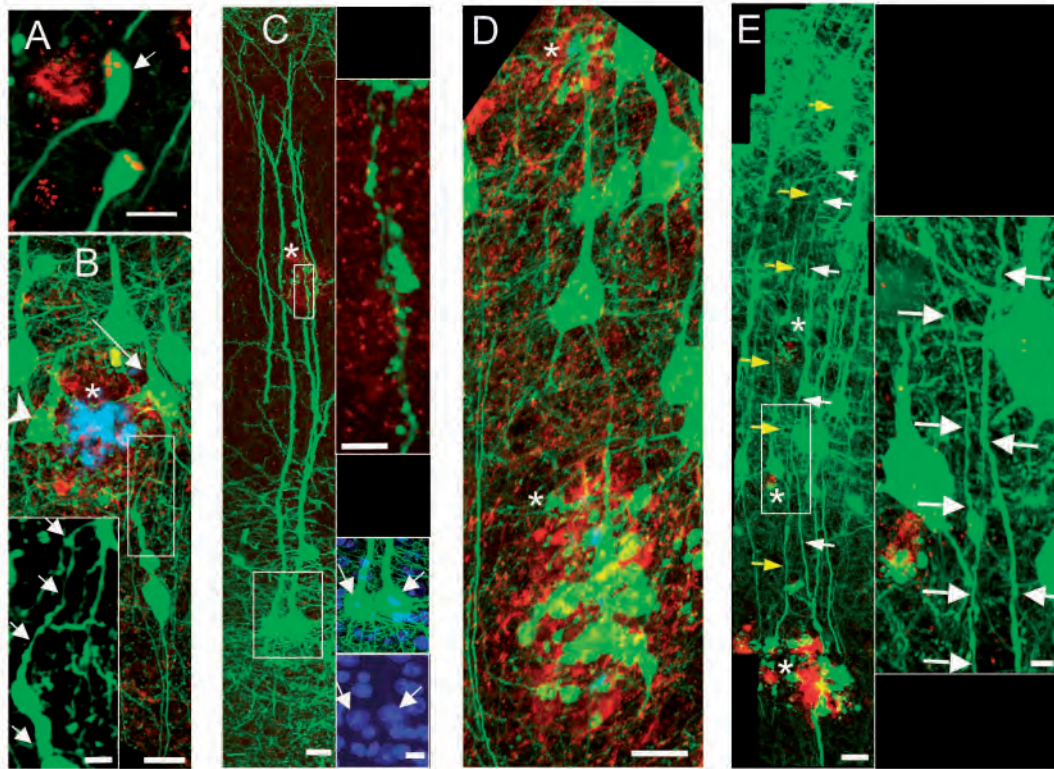


Fig. 8 Heterogeneity of amyloid-associated neuronal damage. (A) Some cell bodies immediately adjacent to amyloid plaques were highly dystrophic (arrow), but note that nuclei were not severely shrunken or misplaced as after axon lesion or transport block (Fig. 1) (see also supplementary figure 10, which shows this more clearly in RGB format) (From a mouse aged 14 months). (B) However, many of these cells also retained axons and dendrites. The boxed area, from a mouse aged 5 months, shows an axon (short arrows) leaving a squashed, plaque-associated neuron (long arrow). The axon is uninterrupted, even though it shows secondary swelling. Another plaque-associated neuron (arrowhead) shows no obvious processes. (C) Dystrophic dendrites (boxed area, top) also retained continuity right up to their apical tufts (top) and down to their cell bodies (boxed area, bottom), here in a mouse aged 4 months. Arrows (inset, bottom) indicate the normal-sized nuclei of the two YFP-H labelled neurons whose apical dendrites are affected by this plaque (asterisk). (D and E) Examples of individual neurons that encounter more than one plaque in a mouse aged 5 months. The neuron in D encounters plaques (asterisk) in its proximal axon and apical dendrite, while E shows two axons (yellow and white arrows, respectively) each encountering three plaques (asterisk) even within their proximal regions. The boxed area is expanded on the right as axon continuity is difficult to follow here on the smaller figure. A, B, D and E: Green = YFP; Red = A β deposits in A, B, C and E; APP staining in D; Blue = Thioflavin S in A and B; Hoechst 33258 dye in C. Scale bar: A: 10 μ m (inset, 5 μ m); B: 20 μ m (inset, 5 μ m); C: 20 μ m (inset, top 5 μ m; inset, bottom, 10 μ m); D, E: 20 μ m (inset, 5 μ m).

There are several indications that our findings are representative also of other models of Alzheimer's disease pathology and the disease in man. In Tg2576 mice, axon density is maintained in the vicinity of plaques, as is density of ascending cortical dendrites above plaques (Spires *et al.*, 2005), and in PDAPP mice, dystrophic neurites are stable for 10–12 h in slice culture and several days *in vivo* (Brendza *et al.*, 2003b, 2005). Our data now show that axonal continuity and cell survival are retained for many months, during which time the reported short-term stability of dystrophic axons gives way to increasing size and complexity (Figs 2 and 3). Although we focussed mostly on axons, the dendrites we observed did not terminate abruptly at plaques (Fig. 8) as reported in PSAPP mice (Tsai *et al.*, 2004). Others also found no dendritic breakage (Spires *et al.*, 2005). Possible explanations include the use of different familial Alzheimer's disease models, and different imaging sites. Distal apical tufts imaged in superficial cortical regions may be more vulnerable than the proximal

dendrites we observed in fixed, sectioned tissue. Perhaps most significantly, the diversion of microtubules into regions of axon dystrophy closely matches that recently described in aged primate brains (Fiala *et al.*, 2007), and the axonal 'diverticula' that are prominent both there and here are very similar in appearance to the dystrophic neurites of human Alzheimer's disease patients (Fischer, 1907). Synapses involving dystrophic axons depleted of synaptic vesicles synapsing onto apparently normal dendrites were also reported in human patients and aged monkeys (Gonatas *et al.*, 1967; Wisniewski *et al.*, 1973; Fiala, 2007). Thus, despite the important differences between transgenic mouse models and human patients, there are strong indications of a conserved mechanism.

Our novel observation of secondary swellings distinguishes two types of axonal dystrophy in Alzheimer's disease like pathology. Primary dystrophy associated with plaques is readily identifiable at 2 months, is largely asymmetric, and reaches huge dimensions

relative to normal axon diameter (Figs 3, 4B and 8D; Supplementary Fig. 1). Secondary swellings, which barely appear before 3 months, are not directly associated with plaques but frequently occur further proximal on the same axons suggesting an indirect relationship. They are usually smaller than corresponding primary swellings and approximately symmetric (Fig. 6), more reminiscent of a block of axonal transport, that may be a cause or an effect of the swelling (Edgar *et al.*, 2004), than of axonal sprouting (Phinney *et al.*, 1999; Park *et al.*, 2006).

Importantly, secondary swelling increases the fraction of axonal length that is dystrophic. We speculate that multiple swellings each add further resistance to axonal transport, resulting in a cumulative effect that is significantly more harmful than the original, single dystrophic region. Thus, this more advanced stage of pathology is likely to increase synaptic dysfunction.

One intriguing possibility for the mechanism of secondary dystrophy is longitudinal, intra-axonal spreading from sites of primary axonal dystrophy, perhaps related to suggestions that intra-axonal A β makes an important contribution to pathogenesis (Wirths *et al.*, 2006). Alternatively, primary and secondary dystrophy could arise by a similar mechanism, perhaps triggered when extracellular A β reaches a threshold concentration. As plaques appear to be surrounded by significant accumulations of soluble A β , this would be expected to occur much sooner in their vicinity and only later at more distant sites, explaining the apparent radial spreading to other areas of the same axon and to its neighbours (Fig. 6D). We also saw occasional secondary dystrophy at more distal sites on the same axon, consistent with a radial spreading mechanism (Supplementary Fig. 3). However, this does not exclude an additional intra-axonal process.

The identification of secondary swellings brings a fresh perspective to the debate about whether dystrophic neurites are confined to the immediate vicinity of amyloid plaques. Some studies found dystrophy only within 15 μ m of plaques (Brendza *et al.*, 2003a; Tsai *et al.*, 2004), but others suggest a plaque-independent population of dystrophic neurites (Braak *et al.*, 1986; Stokin *et al.*, 2005). We now show that dystrophic axons occur as secondary swellings up to 160 μ m from a primary swelling on the same axon. Thus, while not directly associated with plaques, these secondary swellings could yet be a consequence of them. A similar explanation could underlie neuropil threads often seen in human Alzheimer's disease (Nicoll *et al.*, 2003), although we found no structures that were abnormally positive for phospho-tau antibodies. Regarding primary swellings, we found these only in association with plaques but cannot exclude the possibility that some axons not labelled with YFP may have swollen before plaques appeared.

Longitudinal imaging allowed us to view axonal, somatic and dendritic compartments of individual neurons simultaneously and, in doing so, revealed a remarkable heterogeneity of pathology. No two neurons are affected in quite the same way (Fig. 8) suggesting that the route to neuronal dysfunction, and possibly even to cell death, in Alzheimer's disease is not a single pathway. In addition to the many examples of axonal dystrophy that we show, some neurons encounter plaques through their cell bodies and some through their dendrites, causing dystrophy and spine loss. Remarkably even severely misshapen cell bodies are also

sometimes able to support their axon and dendrites for a while (Fig. 8B) and dystrophic dendrites remain continuous and connected to morphologically normal cell bodies (Fig. 8C), mirroring recent findings in ischemia (Enright *et al.*, 2007). Thus, the dysfunction resulting from spine loss and presynaptic swelling is initially highly localised to one compartment. How this eventually leads to irreversible damage and cell death remains unclear, as there seems to be no single, critical compartment in which a plaque causes rapid cell death. This, together with our finding that neurons eventually encounter several plaques, either in different compartments (Fig. 8D) or in the same compartment (Fig. 8E), leads us to speculate that the cumulative effect of many dispersed insults, each individually below the threshold for neuronal death, may eventually become too much for cell to bear. This model offers an intriguing explanation for the absence of significant cell death in mouse models. The far greater length of human axons and dendrites may eventually expose them to damage at a larger number of sites than their murine counterparts. Thus, this 'multi-hit hypothesis' needs to be considered alongside differences such as longevity and isoforms of tau between humans and mice when trying to understand why human neurons die in far greater numbers than those in mice.

We propose that the source of A β is also heterogeneous. Lesioning the perforant pathway input to the dentate gyrus showed clearly that presynaptic endings are one site of release (Lazarov *et al.*, 2002; Sheng *et al.*, 2002), but like others (Wirths *et al.*, 2006) we found plaques in corpus callosum (Supplementary Fig. 5B) and other white matter tracts (data not shown) that lack significant synaptic input. Thus, some A β may have an axonal origin, consistent with the influence of axonal transport on A β generation (Stokin *et al.*, 2005). Non-neuronal origins could also explain these observations.

Many therapeutic strategies aim to reduce A β load by blocking production or enhancing clearance (Nicoll *et al.*, 2003; Hardy, 2006). Immunotherapy in mice causes some dystrophic neurites to disappear (Brendza *et al.*, 2005) but the therapeutic implications of this depend critically upon retained axon and dendrite continuity. Dystrophy could be resolved by recovery of continuous neurites or by degeneration of interrupted neurites but until now information on the length of time that dystrophic neurites remain continuous has been very limited and controversial (Tsai *et al.*, 2004; Spires *et al.*, 2005). Moreover, the fates of the corresponding cell bodies and more distal axon regions have never been reported. Our finding that the overwhelming majority of dystrophic axons remain continuous 4 months after dystrophy first arises, and that other parts of the same cell appear normal, indicates that these cells meet the first requirements for functional rescue. Loss of presynaptic boutons (Fig. 7) should be rectifiable by activating synaptogenesis or sprouting as long as the axon trunk survives. Thus, the therapeutic window for rescuing individual neurons could be considerably longer than suggested by the barely recognisable appearance of dystrophic axons. Intriguingly, human imaging studies using Pittsburgh compound B suggest amyloid deposition occurs long before symptoms arise (Blennow *et al.*, 2006). We speculate that our findings in mice may represent the structural correlate of these stages, where synapse

dysfunction is restricted to local events but long-range axon and dendrite loss, and cell death, have yet to occur.

In conclusion, our data show a clear distinction between local synapse loss and long-range, irreversible degeneration of axons and dendrites in this model for up to 1 year after plaques and dystrophy first arise. Although there are structural synaptic deficiencies locally associated with swollen axons, almost all axons and dendrites retain continuity across highly dystrophic regions up to 6 months and most for up to 1 year, and cell bodies remain capable of supporting these processes. We speculate that neurons may retain the potential for functional recovery for many months after their axons become dystrophic. Pathology is highly heterogeneous at the individual cell level, and multi-site pathology may have important roles in the more advanced stages. These findings raise many new questions about axonal dystrophy that should now be addressed. Do functional synapses remain in the lengthy non-dystrophic regions of affected axons? Do axons and dendrites 'die back' just at their distal ends as a result of axonal dystrophy? Are dystrophic axons able to conduct action potentials? Until what stage can dystrophic axons recover (Brendza *et al.*, 2005)? Does the onset of secondary dystrophy influence the potential for recovery? Are other neuronal subtypes more vulnerable? Is impairment of axonal transport a gradual process, and if so does it feed back into generation of yet more A β (Stokin *et al.*, 2005)? Are dystrophic axons a source of A β , a response to A β coming from other sources or both? And most importantly, can axonal dystrophy or the transport impairment that appears to underlie it be successfully targeted as a therapeutic approach?

Supplementary material

Supplementary material is available at *Brain* online.

Acknowledgements

We thank Prof. Peter St George-Hyslop for the TgCRND8 mouse strain, Prof. Richard Ribchester, Dr Piers Emson and Dr Bogdan Beirowski for helpful discussion, Dr Anne Segonds-Pichon for advice on statistics, Dr Tom Bellamy for additional exploratory work and Mrs I. Kovács for her excellent technical assistance.

Funding

Alzheimer's Research Trust (ART PG/2005/2 to R.A., E.B., L.J.); the Wellcome Trust (069652/Z/02/Z to A.N.); Babraham Institute/BBSRC core strategic (to M.P.C., S.A.W.). Generation of the MitoP mouse strain was supported by a grant from the Dana foundation (to M.K. and T.M.).

References

Adalbert R, Gilley J, Coleman MP. Abeta, tau and ApoE4 in Alzheimer's disease: the axonal connection. *Trends Mol Med* 2007; 13: 135–42.

- Beirowski B, Adalbert R, Wagner D, Grumme D, Addicks K, Ribchester RR, et al. The progressive nature of Wallerian degeneration in wild-type and slow Wallerian degeneration (WldS) nerves. *BMC Neurosci* 2005; 6: 6.
- Beirowski B, Berek L, Adalbert R, Wagner D, Grumme DS, Addicks K, et al. Quantitative and qualitative analysis of Wallerian degeneration using restricted axonal labelling in YFP-H mice. *J Neurosci Meth* 2004; 134: 23–35.
- Bellucci A, Luccarini I, Scali C, Prosperi C, Giovannini MG, Pepeu G, et al. Cholinergic dysfunction, neuronal damage and axonal loss in TgCRND8 mice. *Neurobiol Dis* 2006; 23: 260–72.
- Berkelaar M, Clarke DB, Wang YC, Bray GM, Aguayo AJ. Axotomy results in delayed death and apoptosis of retinal ganglion cells in adult rats. *J Neurosci* 1994; 14: 4368–74.
- Blennow K, Zetterberg H. Pinpointing plaques with PIB. *Nat Med* 2006; 12: 753–4.
- Boutajangout A, Authalet M, Blanchard V, Touchet N, Tremp G, Pradier L, et al. Characterisation of cytoskeletal abnormalities in mice transgenic for wild-type human tau and familial Alzheimer's disease mutants of APP and presenilin-1. *Neurobiol Dis* 2004; 15: 47–60.
- Braak H, Braak E, Grundke-Iqbal I, Iqbal K. Occurrence of neurofilament threads in the senile human brain and in Alzheimer's disease: a third location of paired helical filaments outside of neurofibrillary tangles and neuritic plaques. *Neurosci Lett* 1986; 65: 351–5.
- Brendza RP, Bacsikai BJ, Cirrito JR, Simmons KA, Skoch JM, Klunk WE, et al. Anti-Abeta antibody treatment promotes the rapid recovery of amyloid-associated neuritic dystrophy in PDAPP transgenic mice. *J Clin Invest* 2005; 115: 428–33.
- Brendza RP, O'Brien C, Simmons K, McKeel DW, Bales KR, Paul SM, et al. PDAPP; YFP double transgenic mice: a tool to study amyloid-beta associated changes in axonal, dendritic, and synaptic structures. *J Comp Neurol* 2003a; 456: 375–83.
- Brendza RP, Simmons K, Bales KR, Paul SM, Goldberg MP, Holtzman DM. Use of YFP to study amyloid-beta associated neurite alterations in live brain slices. *Neurobiol Aging* 2003b; 24: 1071–7.
- Bridge K, Berg N, Adalbert R, Babetto E, Dias T, Spillantini MG, et al. Late onset distal axonal swelling in YFP-H transgenic mice. *Neurobiol Aging* 2007 [Epub ahead of print, doi:10.1016/j.neurobiolaging.2007.06.002].
- Capetillo-Zarate E, Staufenbiel M, Abramowski D, Haass C, Escher A, Stadelmann C, et al. Selective vulnerability of different types of commissural neurons for amyloid beta-protein-induced neurodegeneration in APP23 mice correlates with dendritic tree morphology. *Brain* 2006; 129: 2992–3005.
- Chishti MA, Yang DS, Janus C, Phinney AL, Horne P, Pearson J, et al. Early-onset amyloid deposition and cognitive deficits in transgenic mice expressing a double mutant form of amyloid precursor protein 695. *J Biol Chem* 2001; 276: 21562–70.
- Coleman M. Axon degeneration mechanisms: commonality amid diversity. *Nat Rev Neurosci* 2005; 6: 889–98.
- Coleman MP, Adalbert R, Beirowski B. Neuroprotective strategies in MS: lessons from C57BL/Wld (S) mice. *J Neurol Sci* 2005; 233: 133–8.
- Conforti L, Adalbert R, Coleman MP. Neuronal death: where does the end begin? *Trends Neurosci* 2007; 30: 159–66.
- Dickson TC, King CE, McCormack GH, Vickers JC. Neurochemical diversity of dystrophic neurites in the early and late stages of Alzheimer's disease. *Exp Neurol* 1999; 156: 100–10.
- Dong H, Martin MV, Chambers S, Csernansky JG. Spatial relationship between synapse loss and beta-amyloid deposition in Tg2576 mice. *J Comp Neurol* 2007; 500: 311–21.
- Edgar JM, McLaughlin M, Yool D, Zhang SC, Fowler JH, Montague P, et al. Oligodendroglial modulation of fast axonal transport in a mouse model of hereditary spastic paraplegia. *J Cell Biol* 2004; 166: 121–31.
- Enright LE, Zhang S, Murphy TH. Fine mapping of the spatial relationship between acute ischemia and dendritic structure indicates selective vulnerability of layer V neuron dendritic tufts within single neurons in vivo. *J Cereb Blood Flow Metab* 2007; 27: 1185–200.

- Feng G, Mellor RH, Bernstein M, Keller-Peck C, Nguyen QT, Wallace M, et al. Imaging neuronal subsets in transgenic mice expressing multiple spectral variants of GFP. *Neuron* 2000; 28: 41–51.
- Ferguson B, Matyszak MK, Esiri MM, Perry VH. Axonal damage in acute multiple sclerosis lesions. *Brain* 1997; 120: 393–9.
- Ferri A, Sanes JR, Coleman MP, Cunningham JM, Kato AC. Inhibiting axon degeneration and synapse loss attenuates apoptosis and disease progression in a mouse model of motoneuron disease. *Curr Biol* 2003; 13: 669–73.
- Fiala JC. Mechanisms of amyloid plaque pathogenesis. *Acta Neuropathol* 2007; 114: 551–71.
- Fiala JC, Feinberg M, Peters A, Barbas H. Mitochondrial degeneration in dystrophic neurites of senile plaques may lead to extracellular deposition of fine filaments. *Brain Struct Funct* 2007; 212: 195–207.
- Fiala JC, Spacek J, Harris KM. Dendritic spine pathology: cause or consequence of neurological disorders? *Brain Res Brain Res Rev* 2002; 39: 29–54.
- Fischer O. Miliare Nekrosen mit drusigen Wucherungen der Neurofibrillen, eine regelmaße Veränderung der Hirnrinde bei seniler Demenz. *Monatsschr Psychiatr Neuro* 1907; 2: 361–72.
- Fishman PS, Parks DA. Death of transcallosal neurons after close axotomy. *Brain Res* 1998; 779: 231–9.
- Gillingwater TH, Ribchester RR. Compartmental neurodegeneration and synaptic plasticity in the Wld (s) mutant mouse. *J Physiol* 2001; 534: 627–39.
- Gonatas NK, Anderson W, Evangelista I. The contribution of altered synapses in the senile plaque: an electron microscopic study in Alzheimer's dementia. *J Neuropath Exp Neurol* 1967; 26: 25–39.
- Grutzendler J, Helmin K, Tsai J, Gan WB. Various dendritic abnormalities are associated with fibrillar amyloid deposits in Alzheimer's disease. *Ann N Y Acad Sci* 2007; 1097: 30–9.
- Hafezparast M, Klocke R, Ruhrberg C, Marquardt A, Ahmad-Annur A, Bowen S, et al. Mutations in dynein link motor neuron degeneration to defects in retrograde transport. *Science* 2003; 300: 808–12.
- Hardy J. A hundred years of Alzheimer's disease research. *Neuron* 2006; 52: 3–13.
- Hudson CS, Deshpande SS, Albuquerque EX. Consequences of axonal transport blockade by batrachotoxin on mammalian neuromuscular junction. III. An ultrastructural study. *Brain Res* 1984; 296: 319–32.
- Koliatsos VE, Price WL, Pardo CA, Price DL. Ventral root avulsion: an experimental model of death of adult motor neurons. *J Comp Neurol* 1994; 342: 35–44.
- Lacor PN, Buniel MC, Furlow PW, Clemente AS, Velasco PT, Wood M, et al. Abeta oligomer-induced aberrations in synapse composition, shape, and density provide a molecular basis for loss of connectivity in Alzheimer's disease. *J Neurosci* 2007; 27: 796–807.
- LaMonte BH, Wallace KE, Holloway BA, Shelly SS, Ascano J, Tokito M, et al. Disruption of dynein/dynactin inhibits axonal transport in motor neurons causing late-onset progressive degeneration. *Neuron* 2002; 34: 715–27.
- Lazarov O, Lee M, Peterson DA, Sisodia SS. Evidence that synaptically released beta-amyloid accumulates as extracellular deposits in the hippocampus of transgenic mice. *J Neurosci* 2002; 22: 9785–93.
- Martin KR, Quigley HA, Valenta D, Kielczewski J, Pease ME. Optic nerve dynein motor protein distribution changes with intraocular pressure elevation in a rat model of glaucoma. *Exp Eye Res* 2006; 83: 255–62.
- Medana IM, Esiri MM. Axonal damage: a key predictor of outcome in human CNS diseases. *Brain* 2003; 126: 515–30.
- Meyer-Luehmann M, Spires-Jones TL, Prada C, Garcia-Alloza M, de Calignon A, Rozkalne A, et al. Rapid appearance and local toxicity of amyloid-beta plaques in a mouse model of Alzheimer's disease. *Nature* 2008; 451: 720–5.
- Miledi R, Slater CR. On the degeneration of rat neuromuscular junctions after nerve section. *J Physiol* 1970; 207: 507–28.
- Misgeld T, Kerschensteiner M, Bareyre FM, Burgess RW, Lichtman JW. Imaging axonal transport of mitochondria in vivo. *Nat Methods* 2007; 4: 559–61.
- Nicoll JA, Wilkinson D, Holmes C, Steart P, Markham H, Weller RO. Neuropathology of human Alzheimer disease after immunization with amyloid-beta peptide: a case report. *Nat Med* 2003; 9: 448–52.
- Onorato M, Mulvihill P, Connolly J, Galloway P, Whitehouse P, Perry G. Alteration of neuritic cytoarchitecture in Alzheimer disease. *Prog Clin Biol Res* 1989; 317: 781–9.
- Park JH, Gimbel DA, GrandPre T, Lee JK, Kim JE, Li W, et al. Alzheimer precursor protein interaction with the Nogo-66 receptor reduces amyloid-beta plaque deposition. *J Neurosci* 2006; 26: 1386–95.
- Phinney AL, Deller T, Stalder M, Calhoun ME, Frotscher M, Sommer B, et al. Cerebral amyloid induces aberrant axonal sprouting and ectopic terminal formation in amyloid precursor protein transgenic mice. *J Neurosci* 1999; 19: 8552–9.
- Pilling AD, Horiuchi D, Lively CM, Saxton WM. Kinesin-1 and Dynein are the primary motors for fast transport of mitochondria in Drosophila motor axons. *Mol Biol Cell* 2006; 17: 2057–68.
- Pun S, Santos AF, Saxena S, Xu L, Caroni P. Selective vulnerability and pruning of phasic motoneuron axons in motoneuron disease alleviated by CNTF. *Nat Neurosci* 2006; 9: 408–19.
- Rui Y, Tiwari P, Xie Z, Zheng JQ. Acute impairment of mitochondrial trafficking by beta-amyloid peptides in hippocampal neurons. *J Neurosci* 2006; 26: 10480–7.
- Selkoe DJ. Alzheimer's disease is a synaptic failure. *Science* 2002; 298: 789–91.
- Sheng JG, Price DL, Koliatsos VE. Disruption of corticocortical connections ameliorates amyloid burden in terminal fields in a transgenic model of Abeta amyloidosis. *J Neurosci* 2002; 22: 9794–9.
- Spires TL, Meyer-Luehmann M, Stern EA, McLean PJ, Skoch J, Nguyen PT, et al. Dendritic spine abnormalities in amyloid precursor protein transgenic mice demonstrated by gene transfer and intravital multiphoton microscopy. *J Neurosci* 2005; 25: 7278–87.
- Stokin GB, Lillo C, Falzone TL, Brusch RG, Rockenstein E, Mount SL, et al. Axonopathy and transport deficits early in the pathogenesis of Alzheimer's disease. *Science* 2005; 307: 1282–8.
- Teipel SJ, Bayer W, Alexander GE, Zebuhr Y, Teichberg D, Kulic L, et al. Progression of corpus callosum atrophy in Alzheimer disease. *Arch Neurol* 2002; 59: 243–8.
- Tsai J, Grutzendler J, Duff K, Gan WB. Fibrillar amyloid deposition leads to local synaptic abnormalities and breakage of neuronal branches. *Nat Neurosci* 2004; 7: 1181–3.
- Wirths O, Weis J, Kaye R, Saido TC, Bayer TA. Age-dependent axonal degeneration in an Alzheimer mouse model. *Neurobiol Aging* 2006; 28: 1689–99.
- Wisniewski HM, Ghetti B, Terry RD. Neuritic (senile) plaques and filamentous changes in aged rhesus monkeys. *Exp Neurol* 1973; 32: 566–84.